

Indirect Selective Laser Sintered Fully Ferrous Components – Infiltration Modeling, Manufacturing and Evaluation of Mechanical Properties

Phani Vallabhajosyula and David L. Bourell

Laboratory for Freeform Fabrication, Advanced Manufacturing Center

The University of Texas at Austin

1 University Station, MC C2200

Austin TX, 78712-0292

USA

+512-471-3170 voice, +512-471-7681 fax

phani.charana@gmail.com, dbourell@mail.utexas.edu

Abstract Commercially available Selective Laser Sintered (SLS) ferrous components contain copper-based infiltrant in a ferrous preform. The choice of infiltrant has led to inferior mechanical properties of these components limiting their use in many non-injection-molding structural applications, particularly at elevated temperature. In the present work, an attempt has been made to replace the copper-based infiltrant considering cast iron as potential infiltrant for its fluidity, hardness and stability at comparatively high temperature. A critical issue associated with the infiltration was diffusion of carbon from the cast iron into the steel preform thereby decreasing its melting temperature and distorting the part geometry. A predictive model was developed which defines the degree of success for infiltration based on final part geometry and depending on the relative density of the preform and infiltration temperature. The model may be extended to other ferrous powder and infiltrant compositions in an effort to optimize the properties and utility of the final infiltrated part. Initial studies were carried out to validate the model by infiltrating SLSed Laserformtm A6 tool steel preforms with ASTM Type I A532 cast iron. The parts were analyzed for geometry, microstructure and hardness. This research was sponsored by the National Science Foundation under Grant #DMI-0522176.

1. Introduction:

Selective Laser Sintering is a fast growing process for rapid prototyping and rapid manufacturing of functional parts. The process of selective laser sintering suffers from a common deficiency of not being able to produce pore-free parts from many materials. Since porosity diminishes material properties like hardness and ductility, it has to be eliminated as much as feasible. Metal infiltrated metal systems based on selective laser sintering (SLS) have been commercialized for some time [1-5]. Proper infiltrant selection can impart desirable properties to the final part in addition to preserving the part geometry [6, 7]. Selection of bronze infiltrant would lead to a compromise in strength and hardness of the part resulting from generally inferior mechanical properties of bronze compared to those of tool steel [8]. These parts can be used for applications where high thermal conductivity is desired such as short run injection moulds. High temperature stability of ferrous components demands a stable second phase in the ferrous matrix when compared to the commercial (copper based) infiltrant. New infiltrant metals have been considered for which hardness and maximum service temperature are not so severely compromised. In the present work, cast iron is considered as a potential infiltrant for its good fluidity and hardness. Cast iron is also available in a variety of strength grades and microstructures.

This paper deals with modification to the commercial infiltration process whereby a low-melting-point cast iron is substituted for the copper alloy infiltrant. The methodology involves formation of green part as a result of selective laser sintering of LaserFormtm A6 tool steel powder [9-11], burnout of the binder and pre-densification of the component followed by infiltration with cast iron. A critical issue is avoiding melting of the tool steel during infiltration. Diffusion of carbon from the cast iron into the tool steel preform results in lowering of the melting point of the tool steel part significantly. The work was carried out in three stages: constructing a predictive model depending on the relative density of the preform and infiltration temperature to define the degree of success for infiltration based on final part geometry, experimental part generation and analyzing the experimental results by correlating with the model constructed. The experimentation and the resulting parts validation for this model are also discussed in detail.

2. Predictive model for infiltration

To ensure the production of a decent infiltrated part, it is critical to set the infiltration temperature such that the solid fraction at equilibrium does not fall too much below the solid fraction of SLS part prior to infiltration. Preferably the equilibrium solid fraction of the final infiltrated part will be greater than the uninfiltrated tool steel part relative density. The initial density of SLS part prior to infiltration can be varied by sintering the green part at various temperatures.

a) Densification or Ashby plots:

Once the green part is obtained by conventional SLS of the tool steel powder with binder, it is sintered in a vacuum furnace to drive off the binder and create a porous particle network [12]. During the initial stages of sintering coalescence of powder particles occurs by neck formation and growth between the contacting particles. During the intermediate stages particles tend to move closer to one another and the corresponding microstructure is characterized by a tunnel-network of porosity between the particles. Finally the network ceases to exist, giving rise to the formation of isolated spheroidal pores. These pores continue to shrink until the densification is complete. This ensures some hardness to the brown part. The resulting density of the component depends on the initial density, sintering temperature and dwell time at that temperature [13].

Densification of the powder occurs by various mechanisms like plasticity, boundary diffusion, volume diffusion, Nabarro-Herring creep, Coble creep and Power law creep. Ashby, et al. [14, 15] defined densification relations for various mechanisms and created a Temperature Densification Map, a plot of relative density as a function of temperature T. The Ashby plot for densification of LaserFormtm A6 Tool steel with initial relative density of 0.48, approximately, is shown in Figure 1. The resulting relative density for the parts sintered at 1100°C for 3hours and 1260°C for 5hrs is marked by points a, b respectively on the plot.

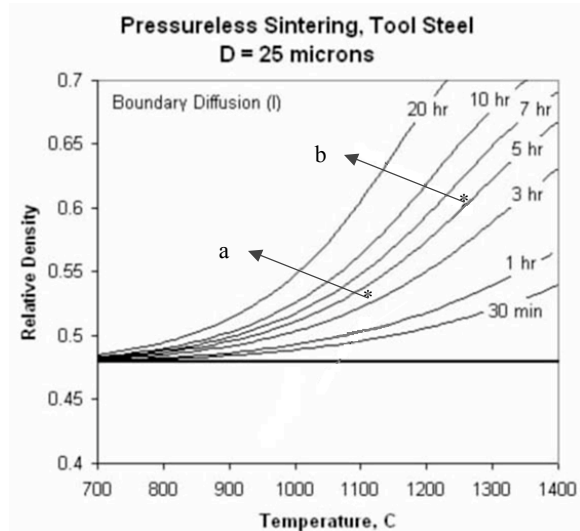


Fig.1. Ashby densification map for tool steel, plotting relative density as a function of temperature and time of sintering. The data points a,b represent increased relative densities of the parts sintered for 3hrs at 1100°C and 5hrs at 1260°C respectively.

b) *Equilibrium solid fraction at infiltration temperature*

Infiltration into the brown part should ensure that cast iron melts completely and diffuses into the brown part without disturbing the part geometry. It was hypothesized that the equilibrium state at infiltration temperature is a mixture of solid tool steel and liquid cast iron. A predictive model for infiltration of cast iron into selective laser sintered tool steel is constructed based on the fact that the equilibrium state at the infiltration temperature is governed by i) carbon content of tool steel and cast iron, ii) infiltration temperature, iii) relative density of tool steel SLS part and iv) amount of infiltrant (excess) needed to ensure complete infiltration.

Let C_i and C_m be the carbon composition of cast iron and tool steel respectively. Considering ρ as the density of pure tool steel and cast iron, if Δ is the relative density of the brown tool steel part, the relative density of cast iron to be infiltrated is given by $1-\Delta$. Let C_e be the equilibrium carbon composition of the resulting part, which may be given by the relation,

$$C_e = [C_m \Delta + C_i(1 - \Delta)] = C_i - \Delta (C_i - C_m) \quad (1)$$

As a reference, Figure 2 shows iron-carbon phase diagram with various materials compositions represented [16]. Let C_L and C_S be the carbon compositions of solidus and liquidus lines at equilibrium which in turn depend on infiltration temperature. The equilibrium solid fraction at the infiltration temperature is given by,

$$X_e = \frac{C_L - C_e}{C_L - C_S} = \frac{[C_L - C_i + \Delta(C_i - C_m)]}{C_L - C_S} \quad (2)$$

Therefore, the equilibrium solid fraction (X_e) at equilibrium state is a function of relative density of the brown part (Δ) and the infiltration temperature (T_i).

This paper deals with infiltration of SLS tool steel part of carbon composition (C_m) 1.09% (wt) with ASTM A532 Class IA white cast iron of carbon composition (C_i) of 3.56% (wt). Based on Equation 2, a graph predicting the equilibrium solid fraction at various temperatures for different relative densities of the brown part is plotted as shown in Figure 3. The dashed line crossing the curves implies the equilibrium solid fraction is equal to the relative density of the brown part at a given infiltration temperature. A point in Region I i.e., above the dashed line represents a higher value of solid fraction than the value prior to infiltration. The cast iron melts and infiltrates into the solid brown part resulting in a decent fully ferrous component. Any point below the dashed line i.e., in the Region II, represents the equilibrium solid fraction to be actually less than the relative density of the brown part. In this case, melting of the part is observed resulting in the distortion of the part.

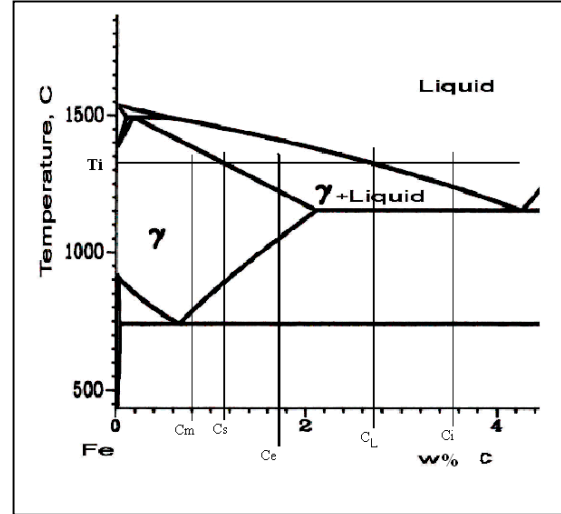


Fig.2. Iron-carbon equilibrium diagram. The definitions for carbon compositions at various points are given in the text.

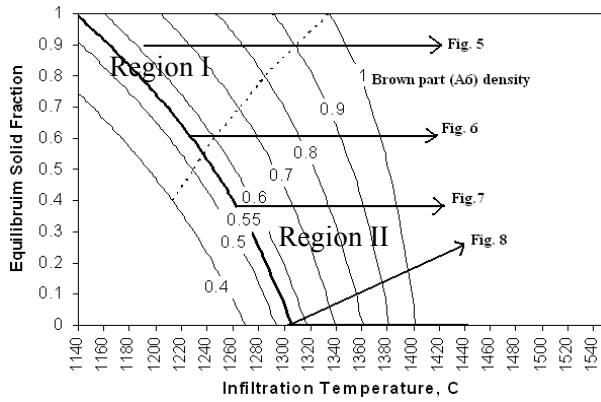


Fig.3. Equilibrium solid fraction as a function of infiltration temperature for different densities of brown part. The data points marked on the plot represent figures of various infiltrated parts; the details are discussed in the text.

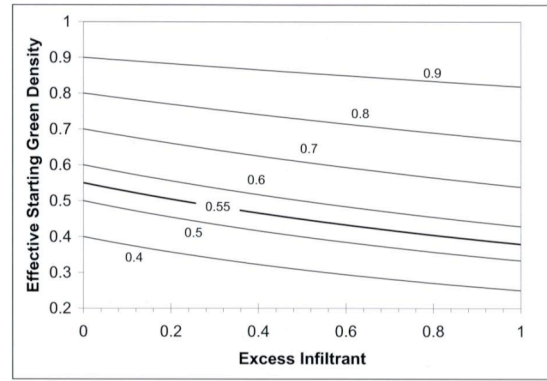


Fig.4. Effect of excess infiltrant on effective starting density for various densities of tool steel brown part. This also results in a decrease of equilibrium solid fraction at infiltration temperature as the amount of infiltrant increases.

c) Effect of Excess Infiltrant

Excess of infiltrant is needed to ensure complete infiltration of the part. Consider an excess of infiltrant (cast iron) be placed on the tabs of tool steel perform during infiltration. This actually alters the effective solid fraction, decreasing it initially. This in turn decreases the equilibrium solid fraction at infiltration temperature. Let ϵ be the fraction of excess infiltrant by volume to the actual volume of infiltrant needed i.e., when ϵ is equal to zero implies the absence of excess infiltrant, and when ϵ equals to 0.2 implies the volume of infiltrant taken is 20% in excess to the actual volume of infiltrant needed. The effective starting density of green part as a function of excess infiltrant is given by,

$$\bar{A}_{\text{eff}} = \frac{\bar{A}}{[\bar{A} + (1 + \bar{a})(1 - \bar{A})]} = \frac{\bar{A}}{[1 - \bar{a}(1 - \bar{A})]} \quad (3)$$

Figure 4 shows the decrease in the effective starting density as ϵ increases. The amount of decrease for a reasonable values of $0 < \epsilon < 0.5$ results in only modest changes to Δ_{eff} of less than 10% approximately.

3. Experimental

Various experiments were carried out to validate the predictive model, in which cubes of dimensions 25mmx25mmx25mm, with a tab for placing the cast iron chunks were built on SLS machine from LaserFormtm A6 tool steel. The green density of these SLS parts was obtained from the ratio of weight of the part to its measured volume. Once the green density was known, the part was buried in alumina and put in a furnace to burn out the binder and pre-densify the part. The part was heated at 90°C/hr to a temperature of 750°C to burn out the binder and then at a rate of 100°C/hr to the set temperature, held at that temperature for certain time followed by furnace cooling. The theoretical relative density of the brown part could be predicted from the Ashby plot by knowing the set temperature and the dwell time. This was compared with the actual relative density of the part calculated from its weight and volume.

The pore volume was obtained from the relative density of brown part and the weight of cast iron needed for infiltration was determined. The tab on the brown part was carefully cleaned

and cast iron chunks were placed on it for infiltration. The assembly was buried in alumina and placed in furnace. The heating rate was set at 100°C/hr up to the infiltration temperature and the sample was held there for 50 min followed by furnace cooling. Infiltration of the brown parts with different relative densities was carried at different temperatures to validate the above model.

4. Testing the infiltrated SLS parts

The parts produced were machined to remove the tab portion and tested for any distortion in the part geometry. Once the parts were found to be geometrically sound, they were then tested for geometry, density, microstructure, hardness, tensile strength and transverse rupture strength.

a) *Geometry and Density*: The density of the part was determined using Archimedes method. For the infiltrated parts without any distortion, density was determined from the ratio of the part weight to its volume calculated from the dimensions. Once the density of the part was known, relative density can be found from the ratio of the actual density to the theoretical density of the fully dense part. (Theoretical density of the full dense part is ~ 7.8 g/cc [9])

b) *Microstructure*: Microstructure of the infiltrated parts was obtained using optical microscopy. Microstructure also aided in determining the amount of porosity in the infiltrated parts.

c) *Hardness*: Rockwell hardness C of the parts was determined. The surface of the parts was polished and indented with a Brale indenter. A preload of 10 kg was applied followed by a 150kg force. The deflection on the scale as indicated by the pointer gave the hardness of the infiltrated part. The hardness was measured at different points on the part to test for the consistency in the value. Knoop micro hardness was also found for different phases present in these parts using 500kgf load and equivalent Rockwell hardness was determined [17].

5. Results and Discussion

Various infiltrated parts were obtained from infiltrating brown parts with different initial relative densities at various infiltration temperatures. The geometry of the resulting parts is discussed.

a) *Geometry and density*

Green parts from SLS station with a relative density of 0.48 were pre-densified in vacuum at a temperature of 1260°C for 5hours, increasing the relative density to 0.62. Depending on this value of relative density, the weight of cast iron needed for infiltration was calculated. Both the part and the cast iron chunks placed on its tabs were buried in Alumina and set for infiltration at 1190°C. The part shown in Figure 5 is the decent infiltrated part obtained as a result. From the predictive model, it can be seen that at this infiltration temperature, the equilibrium solid fraction of the part is greater than 0.62 which implies no melting of brown part and thereby results in an acceptably infiltrated part. The relative density of this part was found to be 0.8. Figure 6 shows another sample, with relative density of brown part being 0.57 and infiltrated at 1230°C. The resulting part with a relative density of 0.64 was sound, thus validating the predictive model.

The part shown in Figure 7 represents a brown part with relative density of 0.5 infiltrated at 1275°C which resulted in melting of tool steel and distorted part geometry. It is evident that selection of infiltration temperature for the given brown part relative density from Region II of the predictive model (Figure 3) resulted in melting of tool steel and distorting the part. The part in Figure 8 also validates the model. Distortion in the final part is observed when a brown part with relative density of 0.52 was infiltrated with cast iron at a temperature of 1310°C. The

predictive model also explains the melting of tool steel as the equilibrium solid fraction at this temperature is found to be less than 0.52.



Fig.5. SLsed A6 tool steel part pre-sintered from a relative density of 0.48 to 0.62 by heating to 1260°C for 5hrs and then infiltrated at 1190°C. The resultant density of infiltrated part was 0.8



Fig.6. SLsed A6 tool steel part pre-sintered from a relative density of 0.48 to 0.57 by heating to 1260°C for 5hrs and then infiltrated at 1230°C. The resultant density of infiltrated part was 0.64



Fig.7. SLsed A6 tool steel part pre-sintered from a relative density of 0.49 to 0.5 by heating to 1160°C for 3hrs and then infiltrated at 1275°C. Melting of tool steel and hence distortion of the specimen is observed as the infiltration temperature for given brown density lies in Region II



Fig.8. SLsed A6 tool steel part pre-sintered from a relative density of 0.46 to 0.52 by heating to 1100°C for 3hrs and then infiltrated at 1310°C. As the infiltration temperature for given brown density lies in Region II, melting of tool steel along with cast iron is observed, distorting the final part.

b) Microstructure

To get an insight into the effect of infiltration on laser sintered parts and the amount of porosity present in these parts, microstructural analysis was carried out. The parts were fine polished and etched with 2% nital for 20 seconds to obtain the microstructure.

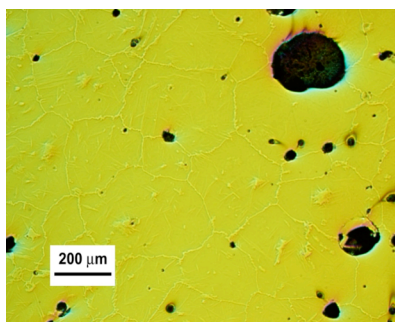


Fig.9. Presence of porosity can be observed from the micrograph (5X) of an unetched component with $\Delta = 0.8$.

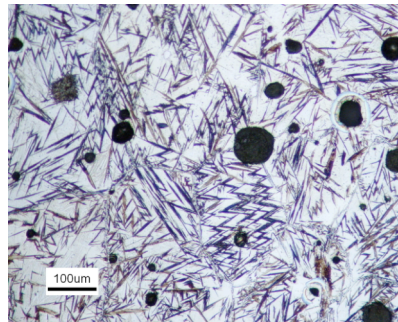


Fig.10. The microstructure of an infiltrated component with $\Delta=0.8$ indicating the presence of porosity and martensite. (10X)

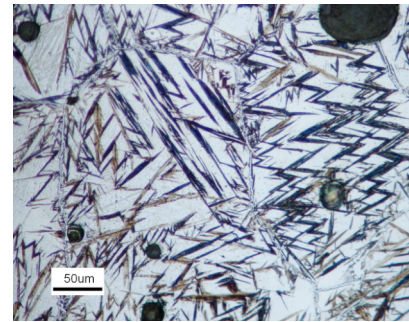


Fig.11. The presence of acicular martensite evident from the microstructure of an infiltrated component with $\Delta=0.8$ (20X)

Considerable porosity is observed from the micrograph of component with relative density 0.8 as shown in Figure 9 and Figure 10. The optical micrographs shown in Figure 10 and Figure 11 indicate acicular martensite in the microstructure. Fine network of cementite is observed to surround the prior formed austenite grains. The presence of martensite imparts hardness to the component, while porosity decreases it significantly.

c) *Hardness*

Rockwell hardness of the polished parts is obtained, and from the hardness values it can be inferred that hardness of the component seems to depend on its relative density, in other words, the amount of porosity. By approaching higher densities for the infiltrated component, it can be possible to achieve higher hardness comparable with that of ASTM A532 white cast iron (53HRC, ASTM Standard).

The general dependence of strength on porosity is given by

$$\sigma = K \sigma_0 (1 - \varepsilon)^m = K \sigma_0 (\Delta)^m \quad (4)$$

where σ is the strength, K and m are constants [18, 19]. The relationship can generally be applied to yield strength, tensile strength and three or four point bend strength. The plot shown in Figure 11 is obtained from Equation 4 and using the porosity and corresponding BHN values observed for the parts. The linear relationship implies that the hardness also varies exponentially with relative density with an exponent of 1.5.

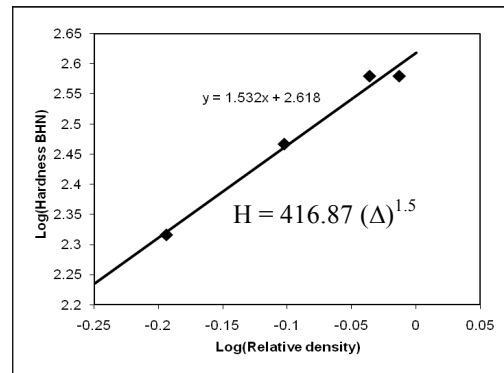


Fig.11. Plot for hardness (BHN) values of infiltrated parts versus their relative density. The linear relationship implies that hardness varied linearly with relative density with an exponent of 1.5.

Micro-hardness: Due to the presence of high porosity, the infiltrated components were tested for micro hardness. Knoop hardness was measured using load of 500kgf. In the region with high density of acicular martensite, the hardness was observed to be 616KHN which is equivalent to 54HRC and the hardness at other region was found to range from 436-500KHN , equivalent to 43-47.2HRC. The high hardness value in the later region can be attributed to the presence of bainite in the microstructure.

6. Conclusions

A predictive model for infiltration of cast iron into SLS tool steel part was developed and tested for different relative densities of brown parts and at various infiltration temperatures. From the above experiments, it was shown that final parts were consistent with the predictive model, and that fully ferrous components can be obtained by proper selection of infiltration temperature for a given relative density of brown part.

The parts obtained should be tested for other mechanical properties like strength and ductility. The predictive model can be further tested considering infiltration with excess infiltrant. Fully dense components might be produced by increasing the number of tabs attached to the part or by adding excess amount of cast iron. The predictive model can be developed further for different ferrous alloys and validated by repeating the experiments at different sintering and infiltration temperatures. The methodology may be tested by first choosing the

product composition for a featured application and working back to determine the required matrix and infiltrant compositions.

ACKNOWLEDGEMENTS

This research was sponsored by the National Science Foundation Grant DMI-0522176

REFERENCES

1. J.J. Beaman, J.W. Barlow, D.L. Bourell, R.H. Crawford, H.L. Marcus, K.P. McAlea, "Solid freeform Fabrication: A New Direction In Manufacturing", Kluwer Academic Press, Boston, 1997.
2. R.B. Heady, J.W. Cahn, "An Analysis of the Capillary Forces in Liquid-Phase Sintering Of Spherical Particles", *Met Trans*, 1970, 1#1, 185-189.
3. F.H. Gern, "Interaction Between Capillary Flow and Macroscopic Silicon Concentration in Liquid Siliconized Carbon/Carbon", *Ceramic Trans*, 1995, 58, 149.
4. B. Stevinson, D.L. Bourell, J.J. Beaman, Jr., "Dimensional Stability During Post-processing of Selective Laser Sintered Ceramic Preforms", *Virtual and Rapid Prototyping*, 1#4, 2006, pp. 209-216.
5. B. Stevinson, D.L. Bourell And J.J. Beaman, Jr., "Over-Infiltration Mechanisms in Selective Laser Sintered Si/SiC Preforms", *Rapid Prototyping Journal*, Vol. 14, 2008, pp. 149-154
6. Stacia L. Barrow, David Bourell, Scott Evans, "An Initial Assessment of Infiltration Material Selection for Selective Laser Sintered Preforms", SFF Symposium, 2004.
7. Adam M. Lorenz, Emanuel M. Sachs, Samuel M. Allen and Michael J. Cima, "Homogeneous Metal Parts By Infiltration", Solid FreeForm Fabrication Symposium, 2001, pp. 69-76
8. S. Kumar, J.P. Kruth, "Effect of Bronze infiltration into Laser Sintered Metallic Parts", *Materials and Design* 28 (2007) pp. 400-407.
9. <http://www.3dsystems.com/>.
10. "Material Guide: Laserform™ A6 Steel Materials", 3D Systems, Inc., Rock Hill SC, 2007.
11. Deckard; Carl R. "Method and apparatus for producing parts by selective sintering" United States Patent #4863538, issued September 5, 1989.
12. David L. Bourell Martin Wohlert and Nicole Harlan, *Deformation, Processing and Properties of Structural Materials*, The Minerals, Metals and Materials Society, 2000.

13. German R.M.(1998) Consolidation Principles and Process Molding in “ASM Handbook Volume 7: Powder Metal Technologies and Applications”, ASM International, Materials Park OH USA, 437-452.
14. M.F.Ashby, “A First report on Sintering Maps”, *Acta Metallurgica*, 22(1974) 275-289.
15. F.B.Swinkels and M.F. Ashby, “A Second Report on Sintering Maps”, *Acta Metallurgica*, 29 (1981) 259-281.
16. ASM Handbook, “Volume 3: Alloy Phase Diagrams”, 10th ed., ASM International, Materials Park OH, 1992, p. 2.110.
17. ASTM E140-07 (2007), “Standard Hardness Conversion Tables for Metals - Relationship among Brinell Hardness, Vickers Hardness, Rockwell Hardness, Superficial Hardness, Knoop Hardness, and Scleroscope Hardness”, American Society for Testing and Materials, Philadelphia, Pennsylvania.
18. German, R.M. (1984) *Powder Metallurgy Science*, Metal Powder Industries Federation, Princeton, New Jersey.
19. Haynes, R., “A Study of Effect of Porosity Content on the Ductility of Sintered Metals”, *Powder Metallurgy*, (1977) Vol. 20, pp. 17-20.